Seismic Interpretation Integrated with Rock Physics and Petrophysical Analysis for the Characterization of 'JAY Field,' Niger Delta

Jallow M.Y.[a*], Oluwadare O. A.[b]

[a,b]*Department of Applied Geophysics, Federal University of Technology Akure, Ondo State, Nigeria*
[a]*Email: muhammedyidhijallow@gmail.com*
[b]*Email: oaoluwadare@futa.edu.ng*

Abstract

Reservoir Characterization involves a holistic approach of describing a reservoir by integrating geologic, geophysical, petrophysical and reservoir engineering using all available data for the characterization of the reservoir's geometric features (including structural and stratigraphic controls) and Petrophysical properties (including porosity, permeability and fluid saturation). The focus is to understand and identify the flow units of the reservoir and predict the inter-well distributions of relevant reservoir properties. JAY field was characterized via Petrophysical analysis, seismic interpretation and modelling, and rock physics analysis. Porosity and permeability models were generated and combined with petrophysical analysis in characterizing the delineated reservoirs. The rock physics cross-plots were used to quality check the results from the seismic and Petrophysical analysis. The structural interpretation of the 3D seismic data of the field revealed anticlinal structures (four-way closure) which is fault assisted and can thus allow hydrocarbon accumulation. Four of the faults are major listric faults that trend in the Northeast Southwest direction. Amongst the remaining fourteen minor faults, five of them are synthetic faults whose sense of displacement is similar to its associated major faults while others are Antithetic faults. Four horizons were established which indicated the top and base of the two reservoirs. The Petrophysical analysis indicated that the reservoirs have good pore interconnectivity (Average $\emptyset_{effective}$= 24% & 21% and Average $K_{average}$ = 9701md & 7737md for Sand A and B respectively).

----

* Corresponding author.

The rock physics analysis confirmed the result obtained from the Petrophysical analysis and furthermore, it showed that the lithologies within the lower portion of the reservoir were partially cemented. Also, the reservoir is found to be predominated by water followed by gas by both rock physics and petrophysical analysis.

Keywords: Seismic interpretation; well logs; Rock physics; Petrophysics.

1.   Introduction

Reservoir Characterization involves a holistic approach to describing a reservoir. By integrating geologic, geophysical (primarily seismic and rock physics method), petrophysical, and reservoir engineering using all available data for the characterization of the reservoir's geometric features (structural and stratigraphic controls) and Petrophysical properties (porosity, permeability, and fluid saturation). The focus is to understand and identify the reservoir's flow units and predict the inter-well distributions of relevant reservoir properties.

To create the most comprehensive reservoir understanding, an integrated reservoir model is increasingly influential. The integrated process compiles petrophysical analysis, seismic interpretation and modelling, rock physics models, and cross plots. The petrophysical analysis is the study of the physical and chemical properties of rocks and their contained fluids. Seismic interpretation involves analyzing seismic data by picking faults and horizons to generate structural maps, reasonable models (such as the porosity, saturation, and permeability models). Predictions about the subsurface properties provide detailed information about how the various reservoir properties vary across the field. Rock physics helps to relate the acoustic behaviour of rocks such as acoustic impedance, Young's modulus, bulk modulus, etc., to measured physical properties within the reservoir. The reservoir parameters such as lithology, pore fluid type, and sediments' cementation can be well understood with rock physics cross plots. The most widely used method in reservoir characterization is Petrophysics, as it provides a direct means of determining reservoir properties. Seismic structural maps and models like the velocity and porosity models were also generated via 3D seismic data and well logs. Using just petrophysical analysis and seismic information to characterize and assess reservoirs' productivity gives a genuinely decisive outcome. To better comprehend how reservoir properties change with estimated seismic properties such as acoustic impedance and velocity, rock physics models, the Gassmann's model, and different cross-plots are utilized together with Seismic models estimated reservoir properties *(petrophysical properties).*

1.1 Geology Of The Study Area

The Niger Delta is situated in the Gulf of Guinea (Figure 2) and extends throughout the Niger Delta Province as defined by Klett and others (1997). From the Eocene to the present, the delta has prograded southwestward, forming depobelts representing the most active portion of the delta at each stage of its development (Doust and Omatsola, 1990) [25]. These depobelts form one of the largest regressive deltas in the world with an area of some 300,000 km2 (Kulke, 1995), a sediment volume of 500,000 km3 (Hospers, 1965), and a sediment thickness of over 10 km in the basin depocenter (Kaplan and others, 1994) [26].

The Niger Delta Province contains only one identified petroleum system (Kulke, 1995; Ekweozor and Daukoru, 1994; this study). This system is referred to here as the Tertiary Niger Delta (Akata –Agbada) Petroleum

System. The maximum extent of the petroleum system coincides with the boundaries of the province (Figure 1) [26]. The minimum extent of the system is defined by the areal extent of fields and contains known resources (cumulative production plus proved reserves) of 34.5 billion barrels of oil (BBO) and 93.8 trillion cubic feet of gas (TCFG) (14.9 billion barrels of oil equivalent, BBOE) (Petroconsultants, 1996a). Most of this petroleum is onshore or on the continental shelf in waters less than 200 meters deep (Figure 1) and occurs primarily in large, relatively simple structures.
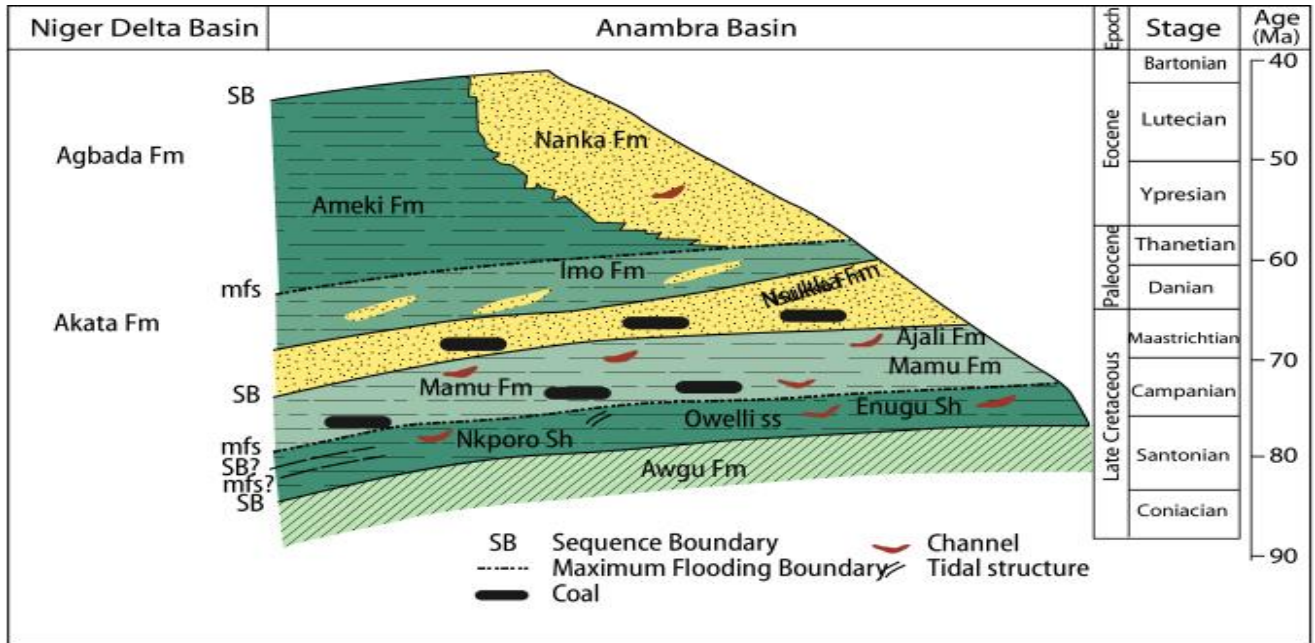
Figure 1: Stratigraphic section of the Anambra Basin. Modified from Reijers and others, 1997
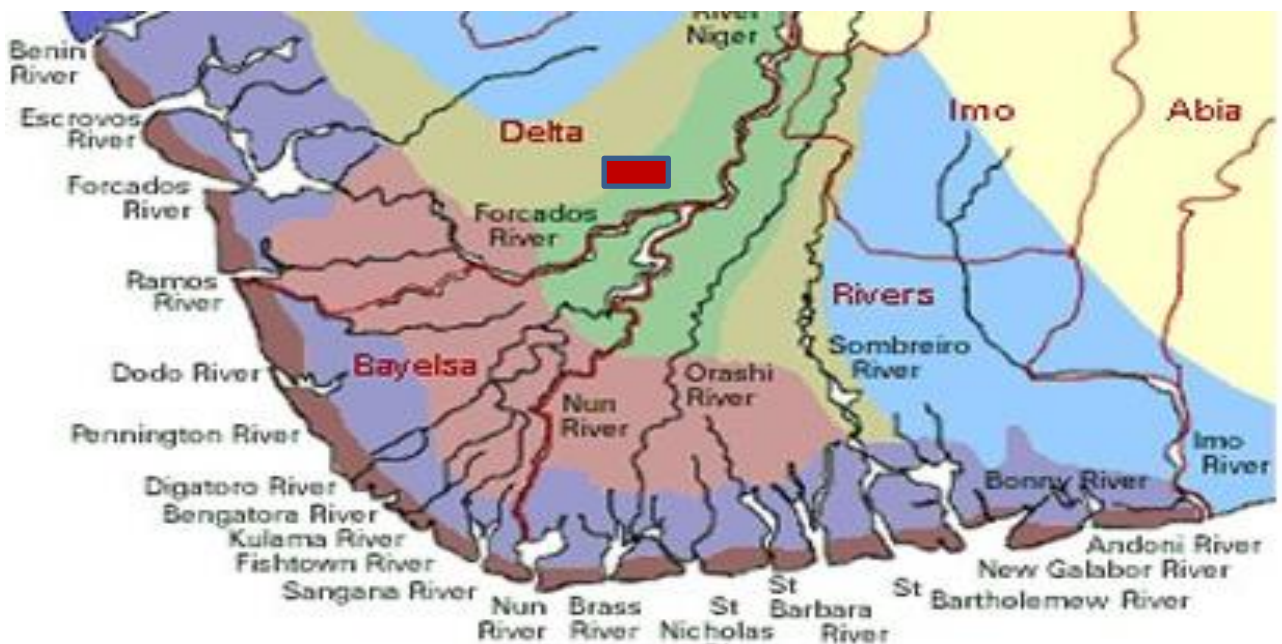
Figure 2: Base map of JAY Field, Niger Delta, Nigeria.
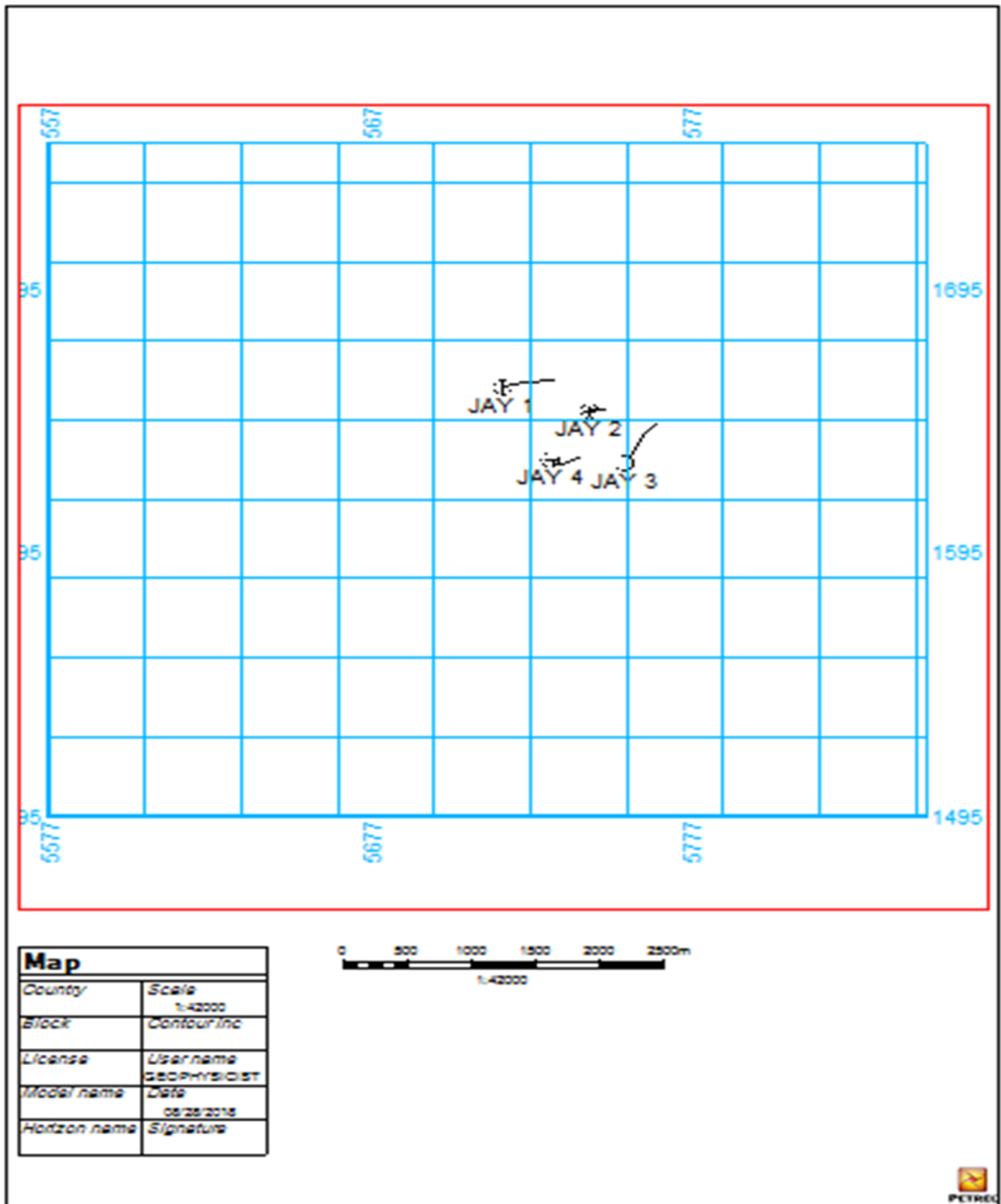
Figure 3: Base Map of JAY Field Showing Seismic Lines and Wells.

A few giant fields do occur in the delta, and the largest contains just over 1.0 BBO (Petroconsultants, Inc., 1996a). Among the provinces ranked in the U.S. Geological Survey's World Energy Assessment (Klett and others, 1997), the Niger Delta province is the twelfth richest in petroleum resources, with 2.2% of the world's discovered oil and 1.4% of the world's discovered gas (Petroconsultants, Inc. 1996a).

The onshore portion of the Niger Delta Province is delineated by southern Nigeria's geology and southwestern Cameroon (Figure 2). The northern boundary is the Benin flank--an east-northeast trending hinge line south of the West Africa basement massif. Outcrops of the Cretaceous define the northeastern boundary on the Abakaliki High and further east-south-east by the Calabar flank--a hinge line bordering the adjacent Precambrian. The offshore boundary of the province is defined by the Cameroon volcanic line to the east, the eastern boundary of the Dahomey basin (the eastern-most West African transform-fault passive margin) to the west, and the two-kilometre sediment thickness contour or the 4000-meter bathymetric contour in areas where sediment thickness is more significant than two kilometres to the south and southwest. The province covers 300,000 km2 and includes the Tertiary Niger Delta (Akata-Agbada) Petroleum System.
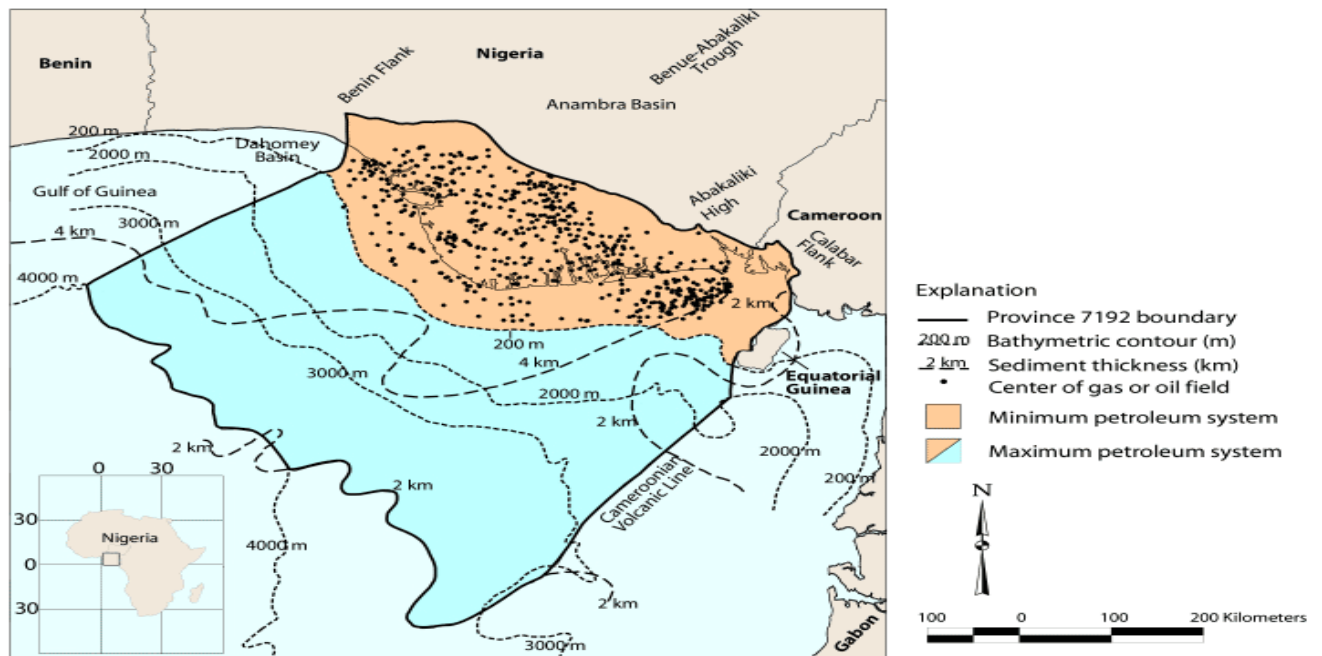
Figure 3: Map of Niger Delta showing Province outline (maximum petroleum system). Data from Petroconsultants (1996a)

2.   Methodology

All the analysis and interpretation carried out during this project research work were done in three different categories with a common goal (to characterize the reservoir). These categories are:

i)   Petrophysical Analysis.

ii)   Seismic Interpretation and Modeling.

iii)   Rock Physics Cross-plots.

2.1   Petrophysical Analysis

The log data (in ASCII format) of all the four wells were loaded into Petrel software and generated curves. Gamma Ray log was placed in Track 1; Resistivity logs were placed in Track 2, while Density and Neutron logs

were placed in Track 3.

2.2   Qualitative Petrophysical Analysis

Observations were first made to identify reservoirs and fluid types.

2.2.1   Delineation of lithologies

Sand and shale bodies were delineated from the gamma-ray log signatures. Sand bodies were identified by a deflection to the left due to the low concentration of radioactive minerals in sand, while deflection to the right signifies shale due to the high concentration of radioactive minerals in it (such as the presence of potassium feldspar in clay minerals).

2.2.2   Fluid Identification

The fluids were identified by using the log signatures of the resistivity logs. Intervals with high resistivity were considered to be hydrocarbon saturated zone while average to low as water resistivity zones as water-bearing intervals.

2.2.3   Well Correlation

The logs were activated and displayed on the well section window, on which correlation was carried out using the lithology log (Gamma-ray log). The resistivity was used to check the fluid contents present within the sediments, i.e., hydrocarbon or water. The top and base of the reservoirs were picked. This process is also known as *lithostratigraphic correlation*.

2.2.4   Fluid Contact Point Identification

Fluid type (oil, gas, or water) was identified using Neutron and Density logs placed on the same track with the neutron log scale reversed. The contact points (cross overs) between these fluids were also identified. Gas usually shows high neutron-density separation, mostly referred to as the *gas effect*.

2.3   Quantitative Petrophysical Analysis

This involved the calculation of various physical properties of the hydrocarbon-bearing sands using Petrel Software. The properties calculated are:

2.3.1   Porosity

Porosity (Φ) is the ratio of pore volume per unit volume of a formation; it is the fraction of the total volume of a sample occupied by pores or voids, usually expressed as a percentage, mathematically it is represented as;

$$\boldsymbol{\Phi_{total}} = \frac{\rho_{ma} - \rho_b}{\rho_{ma} - \rho_f} \qquad\qquad \text{(Eqn. 1)}$$

Where Φ = Total Porosity

ρ$_{ma}$ = Matrix Density

ρ$_b$ = Bulk Density

ρ$_f$ = Fluid Density

2.3.2 Volume of Shale

The gamma-ray log was used to calculate the volume of shale in a porous reservoir. The first step used to determine the volume of shale from a gamma-ray log was the calculation of the gamma-ray index using the equation:

$$I_{GR} = \frac{GR_{log} - GR_{min}}{GR_{max} - GR_{min}}$$ (Eqn. 2)

$$V_{SH} = 0.083(2^{3.7 \times I_{GR}} - 1)$$

Where:

I$_{GR}$ = Gamma-ray index.

GR$_{log}$ = Gamma-ray reading of the formation.

GRmin = Minimum gamma-ray (clean sand).

GRmax = Maximum gamma ray (shale).

VSH = Volume of Shale.

2.3.3 Gross and Net Sand Thickness

The Gross reservoir thickness interval is the interval covering shale and sand within a reservoir. The net thickness of sand is the interval covering only sand within a reservoir. It is called net productive sand. The gross reservoir thickness is determined by knowing the interval covering both sand and shale within the reservoir studied using a gamma-ray log. Net sand thickness is determined by subtracting the interval covering the shale from gross reservoir thickness. Well log data were used in this analysis to generate rock properties using these formulae

GST (Gross sand thickness) = Base of sand - Top of sand

NST (Net sand thickness) = (base + top of sand- shale) if shale is present in the formation, and if not, NST will be the same as GST.

$$\text{NTG (Net to gross)} = \frac{NST}{GST} \qquad\qquad \text{(Eqn. 3)}$$

2.3.4 Formation Factor

The formation factor was calculated from Archie's (1942) equation below;

$$F = \frac{a}{\emptyset^m} \qquad\qquad \text{(Eqn. 4)}$$

Where: Ø= Porosity, a = constant (0.62), m = cementation exponent (2 for sands).

2.3.5 Effective Porosity

These types of porosity values are those corrected for the effect of shale using the formula;

$$\emptyset_{effective} = \left[\left(\frac{\rho_{ma}-\rho_b}{\rho_{ma}-\rho_f}\right)\right] - V_{sh}\left[\left(\frac{\rho_{ma}-\rho_{sh}}{\rho_{ma}-\rho_f}\right)\right] \qquad\qquad \text{(Eqn. 5)}$$

2.3.6 Water Saturation

Water Saturation Sw is the fraction (%) of the pore volume of a reservoir that is occupied by water.

$$S_w = \sqrt{\frac{aR_w}{\emptyset^m R_t}} \qquad\qquad \text{(Eqn. 6)}$$

Sw > 60% wet, Sw from 35% to 60% Marginally wet, Sw < 35% Good potential for hydrocarbon production. Where: Rw is the resistivity of water, Rt is the true formation resistivity and is measured from the log, m is the cementation exponent, and 'a' is a constant.

2.3.7 Hydrocarbon Saturation

This is the percentage of pore volume in a formation occupied by hydrocarbons. It was obtained by subtracting the value obtained for water saturation from 100%.

$$S_h = (1 - S_w)\% \qquad\qquad \text{(Eqn. 7)}$$

2.3.8 Irreducible Water Saturation

This is the water held in the pore spaces by capillary forces. When a zone is at irreducible water saturation (Swirr), the water saturation in the uninvaded zone (Sw) will not move because it is held in grains by capillary pressure. For most reservoir rocks, irreducible water saturation ranges from less than 10% to more than 50% (Schlumberger, 1979). It can be determined from the equation given below.

$$S_{wirr}\sqrt{\frac{F}{2000}} \qquad\qquad \text{(Eqn. 8)}$$

2.3.9   Movable Hydrocarbon Index (MHI)

The movable hydrocarbon index (MHI) was derived using:

$$\text{MHI} = \frac{S_w}{S_{XO}} \qquad \text{(Eqn. 9)}$$

MHI > 1 implies that hydrocarbon is immovable during the invasion, and MHI < 0.7 implies that hydrocarbon was is movable during the invasion. The parameters Sw and Sxo are water saturation of the uninvaded zone and the flushed zone, respectively.

2.3.10   Permeability

Permeability is the ability of a rock to transmit fluid. It is related to porosity but not always dependent on it. It is also controlled by the connecting passages' size (pore throats or capillaries) between pores. Permeability is measured in darcies or millidarcies.

$$K = \sqrt{\frac{250\emptyset^3}{S_{wirr}}} \qquad \text{(Eqn. 10)}$$

Where: K is the permeability, $\emptyset$ is the porosity and S_{wirr} is the irreducible water saturation.

2.3.11   Bulk Volume Water

Bulk volume water is the product of a formation's water saturation (Sw) and its porosity.

$$BVW = S_w \times \emptyset \qquad \text{(Eqn. 11)}$$

2.4   Seismic Interpretation and Modelling

This section of the research work focused on interpreting the available seismic volume. The various geologic structures observed on the field were mapped and then interpreted. Then, structural maps were generated. After that, some petrophysical properties calculated were then modelled to observe their distribution across the reservoirs. The entire operations carried out in this portion of the work were done using Petrel Software.

2..4.1   Fault Interpretation

A fault can be defined as a fracture along which vertical displacement has occurred. This could be a lateral or vertical movement of any part of the rock unit caused by varying tectonic processes. In mapping the faults for this project, the factors considered include:

i)   Abrupt termination of the primary event.
ii)   Displacement along a primary event.

The identification of prominent features such as major and minor faults was carried out on the seismic section, and both major and minor faults were picked on the inlines with the aid of some attributes (Amplitude gain control (AGC), structural smoothening, and variance edge). All the faults mapped are normal faults, and their characteristics showed that of a growth fault.

2.4.2   Well-Seismic Tie (Synthetic Seismogram, Checkshots)

This process (Well-Seismic Tie) was carried out for two main reasons. First, to show that the horizons to be picked on the seismic sections are accurate and correct representatives of those reservoir tops picked on the well logs (based on good petrophysical characteristics). Secondly, it was used to relate geologic events on the well logs in-depth to the same events on the seismic in time.

Synthetic seismograms bridge geological information (well data in depth) and geophysical information (seismic in time). This essentially involves a two-step process:

i)   Time converting the wells utilizing check shot data and sonic logs.
ii)   Generating synthetic seismograms from density logs, sonic logs, and a seismic wavelet by calculating acoustic impedance and reflection coefficients are then convolved using a wavelet.

A 3D seismic cube was sampled along the well path and displayed next to the synthetic seismic to obtain a correlation. Any changes to the time-depth relationship can be made, and seismic horizons can be correlated with the well logs' stratigraphic boundaries.

2.4.3   Horizon Interpretation

A horizon is a surface separating two different rock layers. The surface is identified by a distinctive reflection pattern that can be observed over a layer with a relatively large extent. Identification of prospective sand is from the composite logs available. In an area without well control, strong reflection on the seismic section can be selected for mapping. Time to depth conversion was done, and the corresponding depth structure map was produced.

2.4.4   Map/Surface Making (Time and Depth)

The surface was produced from the horizons mapped from the seismic section, and check shot data was utilized to convert the reservoir top and base in the JAY field in time to depth.

2.4.5   Fault Modelling

The fault modelling process is done by applying manual based techniques of isolating faults by interpreting fault zones of interest in the seismic sections that are correspondingly used to create fault pillars and patches needed in the model. The process of modelling fault planes in a three-dimensional framework defines the geological

model's faults, which will form the basis for generating the 3D grid. These faults will define breaks in the grid lines along which the horizons inserted later may be offset. The offset that occurs depends on the input data, so modelling reverse faults is just as easy as modelling normal faults.

2.4.6   Pillar Gridding

This represents the faults in a 3D grid system, a horizontal and vertical network used to describe a three-dimensional geological model. The final structural modelling is in creating 3D structural grid surfaces, which comprise both the fault modelled pillar grids/models and the horizon surfaces. The base's skeletal framework, mid and top skeletons, are inputted with the edges that provide the structural frame as geo-modelling grids. This process converts the interpreted faults from the fault modelling workflow into pillars in a 3D structural grid surface or model frame. Whether vertical, curve and listric, the nature of fault planes' options is essential to maintain the pillar's fault's structural interpretations.

2.4.7   Vertical Layering

This is the creation of Stratigraphic horizons and subdivisions, i.e., Sub-zonation of a 3D grid. The vertical layering process consists of four steps; Make horizons, Depth conversions, make zones, and Make layers.

2.4.8   Property Modeling

The 3D static models from the JAY seismic data's structural modelling workflow's interpreted reservoir surfaces are populated with discrete properties from inputted well logs to understand each reservoir's property distribution and heterogeneity. The property modelling workflow in this study consists of well Upscaling, data analysis, and Petrophysical modelling.

2.4.9   Scale-Up-Well Logs

When modelling different properties, the modelled area is divided up by generating a 3D grid. Each grid cell has a single value for each property. As the grid cells often are much larger than the sample density for well logs, well log data must be scaled up before they can be entered into the grid. This process is also called blocking of well logs.

All log values that fall within the cell will be averaged according to the selected algorithm to produce one log value for that cell for each grid cell. The resulting 3D grid will only hold values for the wells' 3D grid cells. The well log upscaling process is required to post values in each cell of the 3D grid where each of the wells is situated; average well properties are used to populate each of the cells. This makes it possible to relate the well properties to the grid directly, and this also means that the upscaled cell's properties value along the well path will be static in the whole of the 3D grid property with the upscale zones.

2.4.10   Data Analysis

Data analysis is a quality control process, exploring the data to identify key geological features and prepare inputs for facies and Petrophysical modelling.

2.4.11 Petrophysical Modeling

This process involves modelling some petrophysical parameters such as porosity, permeability, water saturation, net to gross, and defining the fluid contact. It is the process of using petrophysical assigned properties values or attributes as a basis of modelling. The primary input is the facies with the sand and shale attributes, which provides a petrophysical distribution of the sand to shale ratio.

2.5 Rock Physics

This portion of the research work was carried out to quality check the results gotten from the petrophysical analysis, seismic interpretation, and modelling of the two reservoirs delineated across the four wells. It was also used to characterize the reservoir. Various elastic parameters were generated to carry out this work properly and were then cross-plotted against some calculated reservoir parameters.

2.5.1 Calculation of Parameters

Unavailable parameters such as acoustic impedance, primary and secondary velocities that were essential in carrying out the rock physics aspect were calculated via the following formulas:

$$V_p = \left(\frac{1000000}{DT_c} \right) \times 0.3281 \qquad \text{(Eqn. 12)}$$

$$AI = V_p \times \rho_b$$

$$V_s = \frac{V_p - 1279.08}{1.11702} \qquad \text{(Eqn. 13)}$$

Where VS = Primary Velocity, DTC = Compressional Sonic log, AI = Acoustic impedance, ρ = Density from bulk density log and VS = secondary velocity.

2.5.2 Creating Rock Physics Template

Before any cross-plot is done, one needs to examine if the available Rock Physics Templates fit the available well data and the interpretations made from the cross-plots produced based on this template. This refers to a general reference chart for interpreting rock physics cross-plot within a field that cooperates with some diagenetic and depositional trends to describe how lithologies and hydrocarbons vary with depth. This technology was first presented by Odegaard and Avseth (2003).

A rock physics template was created for this field via Rock Doc software and Microsoft Excel.

2.8   *Analysis of Rock physics Template*

Rock physics templates include various rock physics models (including models, contact models, bounds, or relations) based on the interpretations to be made. Rock physics templates are then analyzed based on the well logs and seismic data. These templates are dependent on the sedimentary basin being analyzed.

Based on well Log Data;

The Templates are analyzed and validated for the well logs available. These templates can be used further to predict the lithologies and fluids within that field if they match. If no available template is suitable for the logs, then the templates should be updated. Also, the log quality should be verified as this could impair the quality of the results gotten from the interpretation of the cross plots done on such a faulty template. The last step involves using the right Rock physics Templates to cross-plot Seismic and Reservoir properties.

Based on Seismic Data;

Cross-plot the necessary and needed parameters on the Rock Physics Template. The trends gotten from the cross-plot should be interpreted based on the models used in creating the templates. If the trends gotten from the cross-plot do not match the models, the procedure used in getting the cross-plotted parameters should be adequately checked.

2.9   *Cross Plotting of Elastic and Reservoir Parameters*

Cross-plots of various elastic parameters against some calculated reservoir parameters were then done to quality check the petrophysical analysis, seismic interpretation, and seismic models to produce a dependable result. To no small extent, these plots are useful in making conclusive interpretations of seismic and petrophysical analysis. They show to no small extent the trends in seismic, petrophysical, and geologic parameters altogether.

3.   Results and Discussion

Eleven petrophysical parameters were evaluated for the two delineated reservoirs. The parameters are the volume of shale, porosity, effective porosity, water saturation, hydrocarbon saturation, irreducible water saturation, flush zone water saturation, formation factor, permeability, movable hydrocarbon index, and a bulk volume of water. These properties within the two reservoirs were averaged and displayed in the table below (Table 1).

From the petrophysical analysis carried out in SAND A, the most productive wells are wells JAY1 and JAY4. Of the two wells, JAY1 is thicker but has a higher water saturation and is thus wetter than JAY4. Though their permeability values are high (above 2500md), JAY4 could be more productive. In SAND B, wells JAY1 and JAY4 were observed to contain more hydrocarbon than other wells (i.e., 21% and 11%, respectively) across the four wells. Well One has a lower porosity, which makes it less producible. However, their permeabilities are of the same range.

Sand A

Sand A cuts across four wells (JAY1, JAY2, JAY3, and JAY4) and is overlain by a shale formation that acts as a seal. It has a gross thickness ranging from 17m to 70m, and its net thickness also ranges from 16m to 68m. The average gross thickness and net thicknesses are 34m and 32.3m, respectively.

The average porosity is 26%, the average effective porosity is 24%, with a minute average volume of shale of 0.109units. The water saturation across the four wells in the study area ranges from 45% to 97%, with an average of 70%, which indicates that this reservoir is wet.

The average irreducible water saturation was found to be 8%. This reservoir's hydrocarbon saturation ranges from 3% to 55% and with an average value of 29%. The flush zone water saturation ranges from 81% to 99% while having its average to be 89%. The average movable hydrocarbon index is 0.78, which implies that the hydrocarbon is movable during production. The average permeability of this reservoir is 9701md, and the bulk volume water of the reservoir has an average value of 0.179.

Sand B

Sand B cuts across the four wells (JAY1, JAY2, JAY3, and JAY4) and is overlain by a shale formation that acts as a seal. It has a gross thickness ranging from 99m to 145m, and its net thickness also ranging from 83m to 104m. The average gross and net thicknesses are 123m and 102m, respectively. The average porosity is 23%, the average effective porosity is 21%, with a minute average volume of shale 0.10 units.

This reservoir has its water saturation across the three wells in the study area ranging from 79% to 93%, with an average of 90, which implies that the reservoir is wet. The average irreducible water saturation was found to be 10%.

This reservoir's hydrocarbon saturation ranges from 3% to 21%, with an average value of 11%. The flush zone water saturation ranges from 92% to 97%, with an average of 95%. The average movable hydrocarbon index is 0.866, which implies that hydrocarbon is movable during production. Also, the average permeability of the reservoir is 7737md. The bulk volume water of this reservoir has an average value of 0.187.
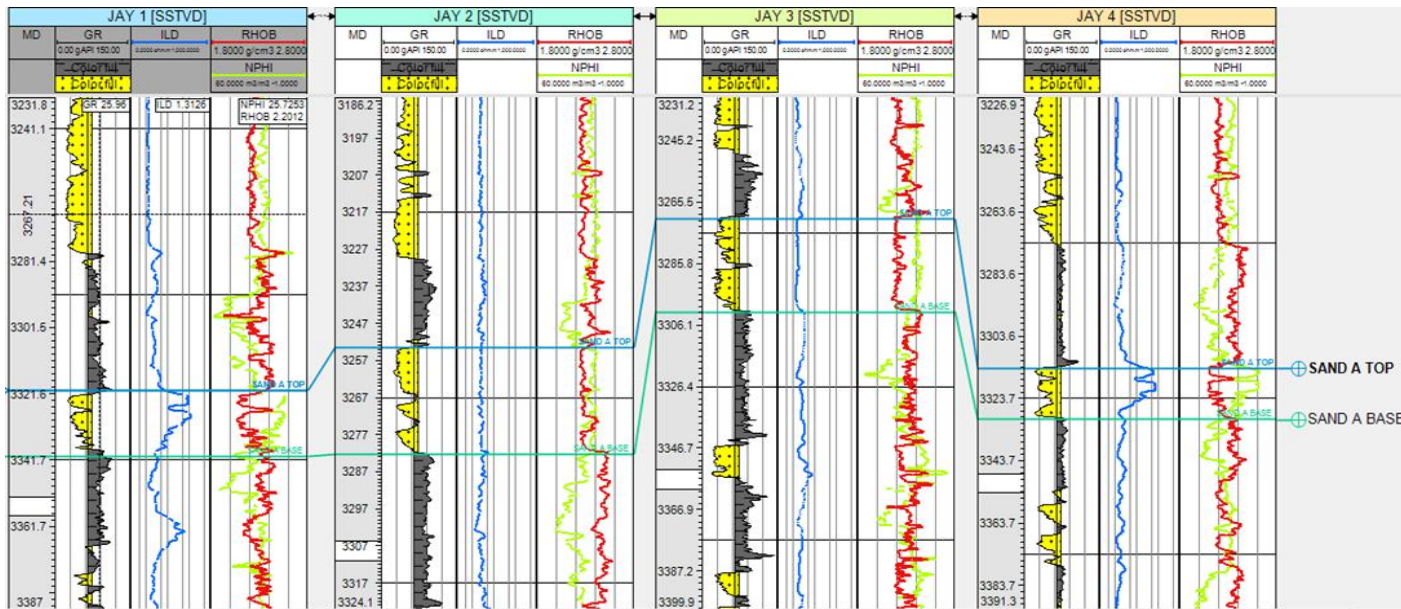
Figure 4.1: Wells Correlated Showing the Top and Base of Sand A Reservoir.
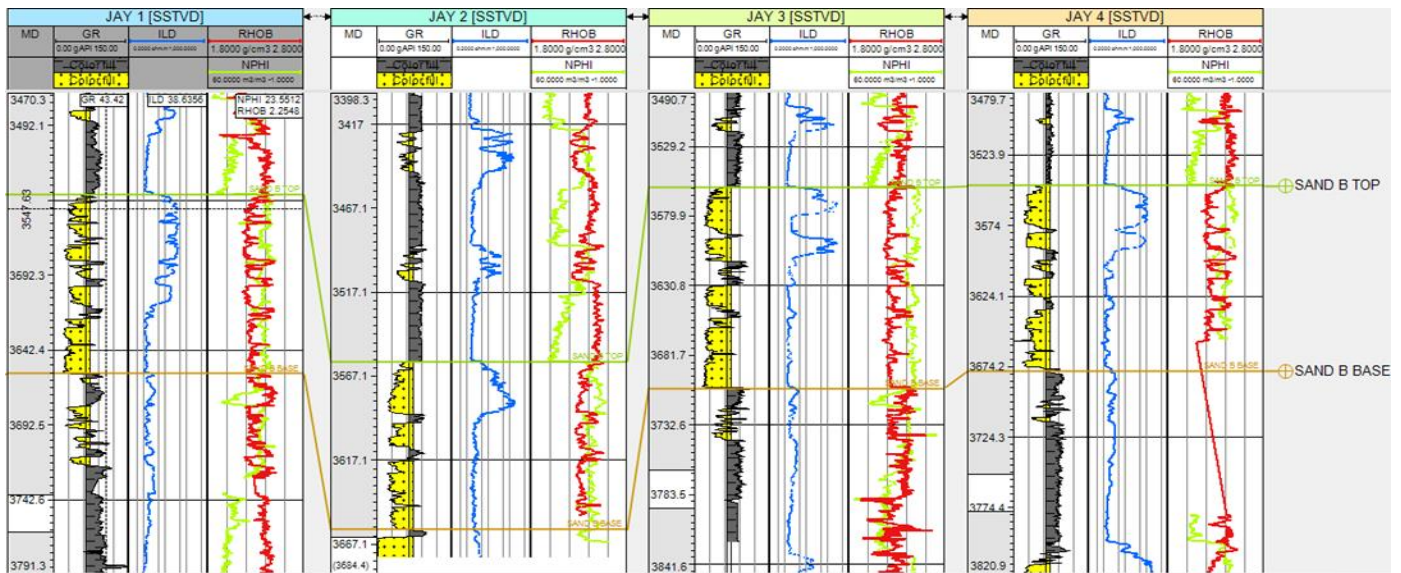
Figure 4.2: Wells Correlated Showing the Top and Base of Sand B Reservoir.

Table 1: Summary of the average computed petrophysical parameters obtained for Sand A&B

Reservoir	Top(m)	Base (m)	Gross (m)	Net (m)	N/G	Porosity (%)	Effective porosity (%)	Sw (%)	Sh (%)	Vshale	Ka (md)
Sand A	3289.59	3313.59	34	32.2	0.93	26	24	71	29	0.109	9701
sand B	3289.59	3313.59	123	102	0.825	23	21	90	11	0.101	7737
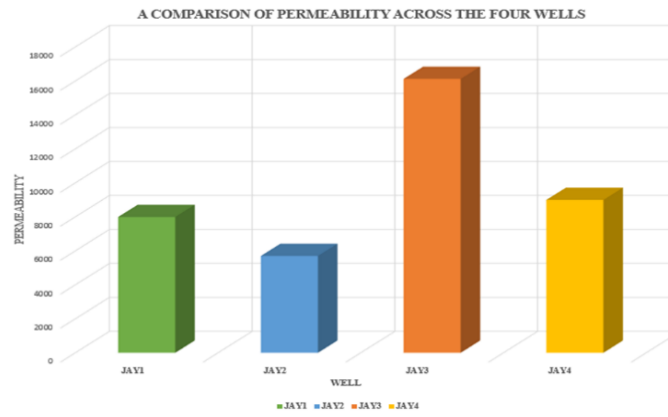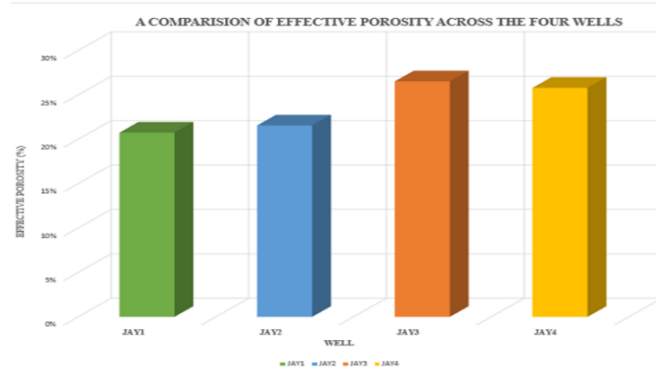
(a) Effective Porosity   (b) Permeability
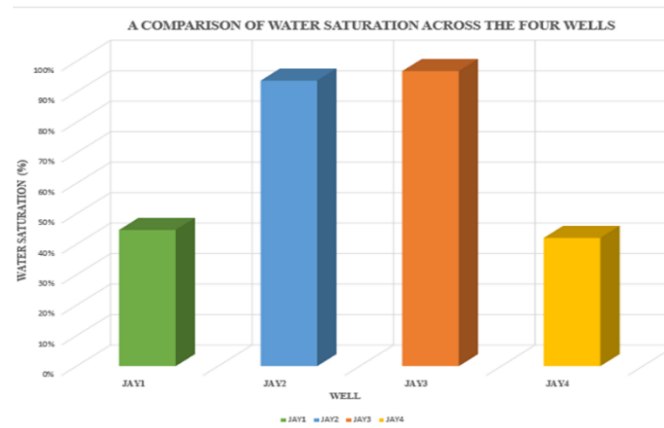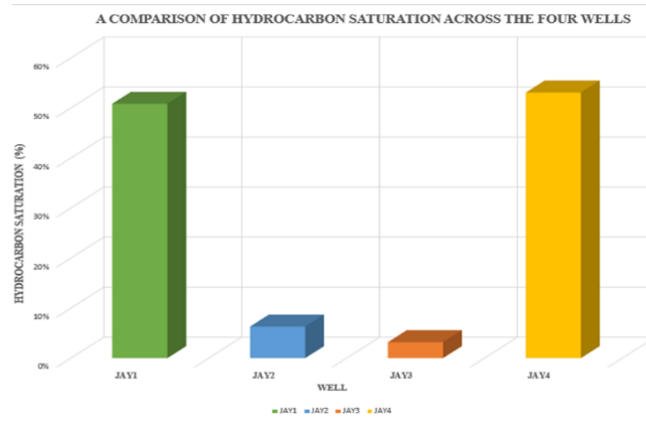
    (c) Water Saturation   (d) Hydrocarbon Saturation

Figure 5: A Bar Chart Showing (a) Effective Porosity Distribution (b) Distribution of Permeability (c) Water Saturation (d) Hydrocarbon Saturation of Sand A.
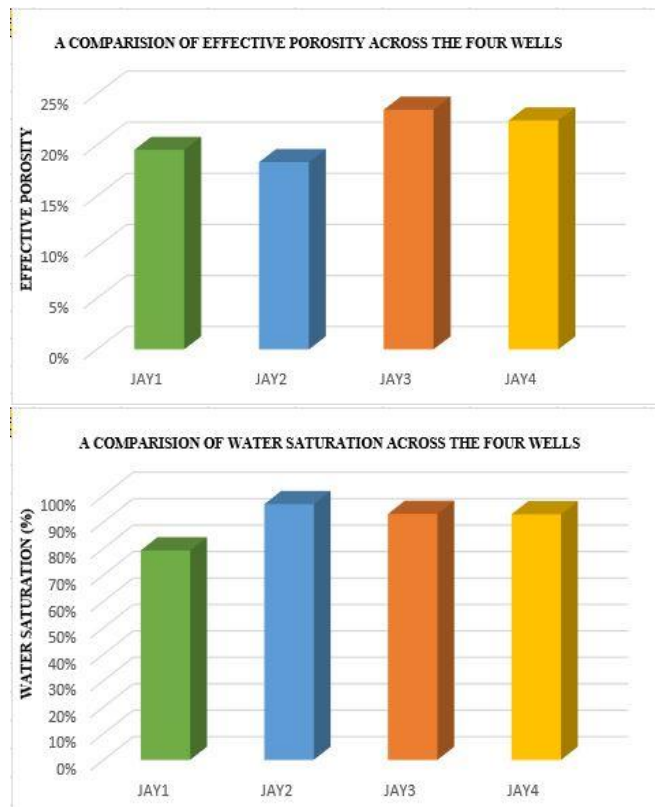
    (a) Effective Porosity   (b) Water Saturation
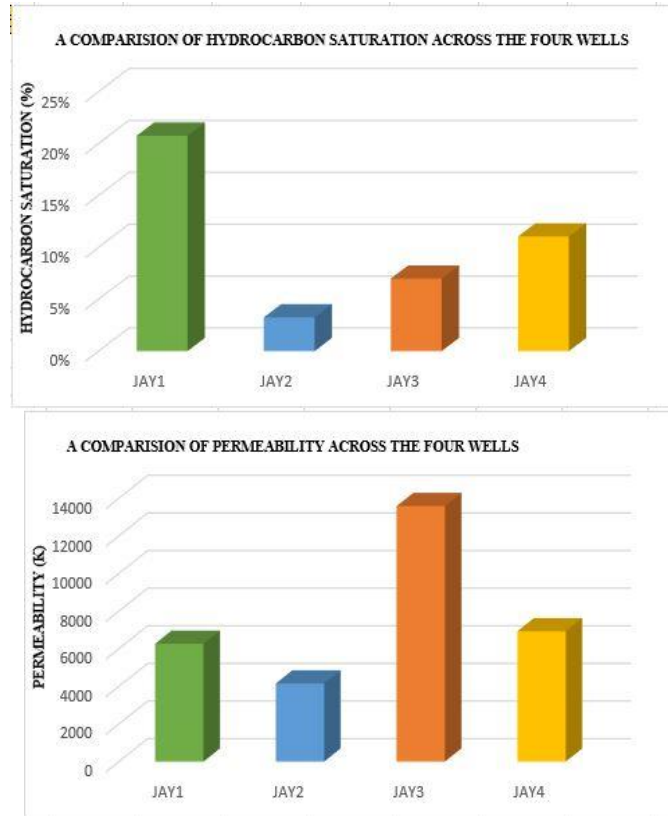
(c) Hydrocarbon Saturation   (d) Permeability

Figure 5: A Bar Chart Showing (a) Effective Porosity (b) Water Saturation (c) Hydrocarbon Saturation (d) Permeability of Sand B.
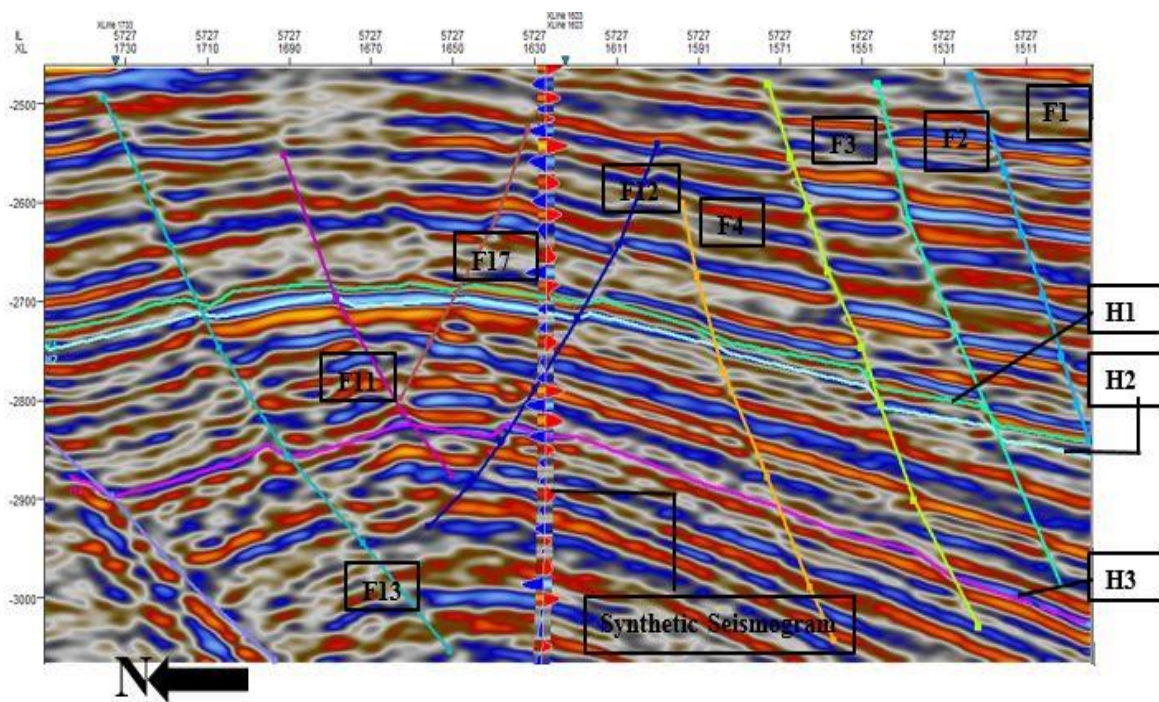
Figure 6: Seismic Section (inline) Showing Mapped Faults, Synthetic Seismogram, and Horizons.

229

3.1   Reservoir Classification

The summary of the average results of the essential petrophysical parameters utilized as variables that determine reservoir quality is presented (Table 1.) above. These parameters are subjected to statistical analysis by considering their values across all the delineated reservoirs in the four wells of the study area and were used to rank the reservoir. The three reservoirs have been classified using the average results of petrophysical parameters. Furthermore, based on these, Sand A is most prolific than Sand B in the JAY field.

3.2   Seismic Interpretation and Modelling

The seismic volume was interpreted, and some petrophysical parameters were modelled. Maps were generated after faults were picked, a synthetic seismogram (Figure 6 above) was generated to relate the seismic data to the well data, and horizons were then picked. The generated maps displayed high and low structural closures, and the models revealed the distribution of the properties across the wells.

3.2.1   Mapped Faults and Horizons

The structural interpretation of the 3D seismic data of the JAY field revealed a total of eighteen faults. Four of the faults (F1, F2, F3, and F4) are major listric faults that are trending in the Northeast Southwest (NE-SW) direction, as shown in Figure 6 above.

Among the remaining fourteen minor faults, five of them are synthetic faults (F5, F7, F8, F11, and F13) whose sense of displacement is similar to its major associated faults and trending in the Northeast Southwest (NE-SW) direction. The remaining mapped faults (F9, F10, F12, F14, F15, F16, and F17) are Antithetic faults whose sense of displacement is opposite to its associated major and synthetic faults having a Southeast Northwest (SE-NW) structural trend.

Four horizons were established, which indicated the top and base of the two reservoirs A (H1 and H2) and B (H3 and H4), respectively, as shown in Figure 6 above.

3.2.2   Structural Maps

These maps were interpreted similarly to the time maps. Structural features revealed on the time maps are also visible here. However, the units of measurement are different. The depth map is in meters, while the time map is in milliseconds (ms).

The southern parts of the maps are bounded by the most dominant faults (F2, F3, and F4), which trend in the northeast South-West direction. Below these significant faults in the southern part of the map, areas of higher depths (cyan to purple) are revealed. This implies that this portion is the downthrown part of the growth faults. This map thus provides information to the drilling engineers. The most profound areas on the map are about 3520m, while the shallow portions on the map lie at a depth of about 3240m. The same structural highs (orange) revealed on the time map are also visible here in the map's North-West central portion. This closure is diagnostic

of an anticlinal structure that could act as a structural trap that could aid hydrocarbon accumulation.

3.2.3   *Petrophysical Modeling*

The porosity and permeability estimated across Sand A were modelled (Figure 7c & 7d). This shows the distribution of these parameters away from the well locations across Sand A. Combining these Petrophysical models and the generated maps, other hydrocarbon prospects were identified.

(a)   (b)

(c)

(d)
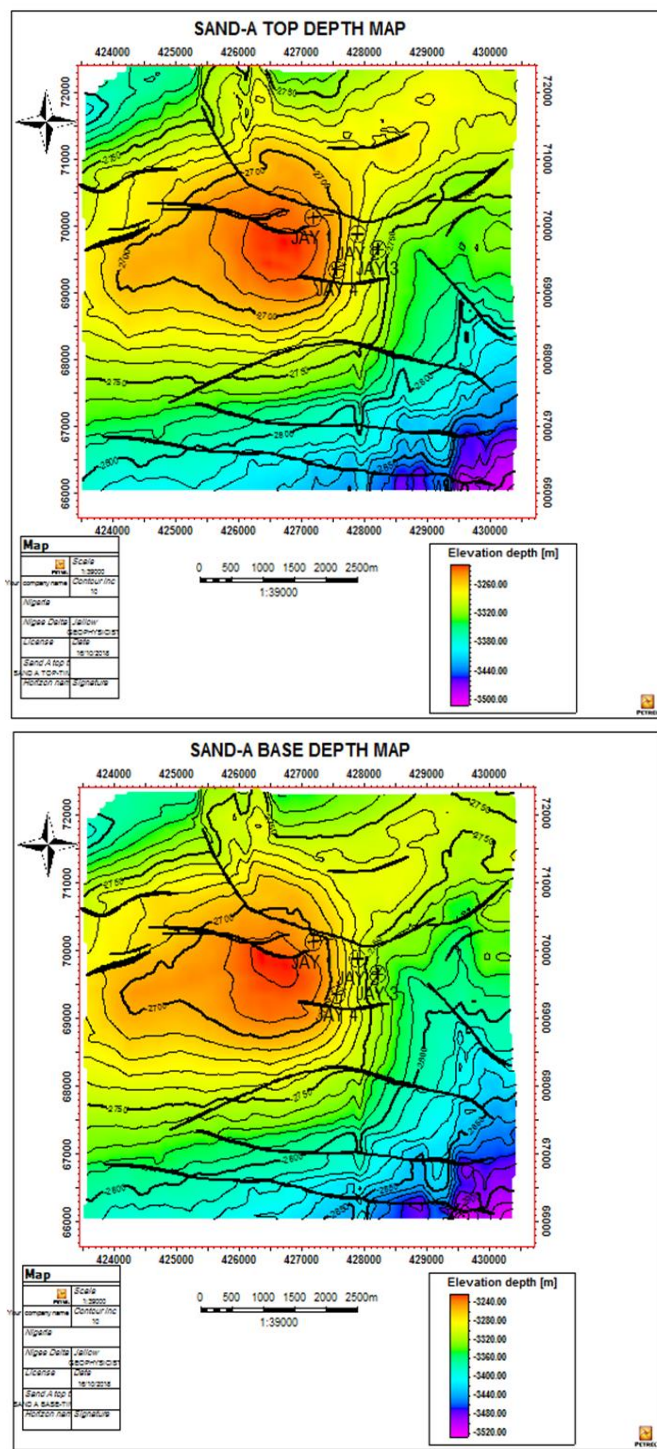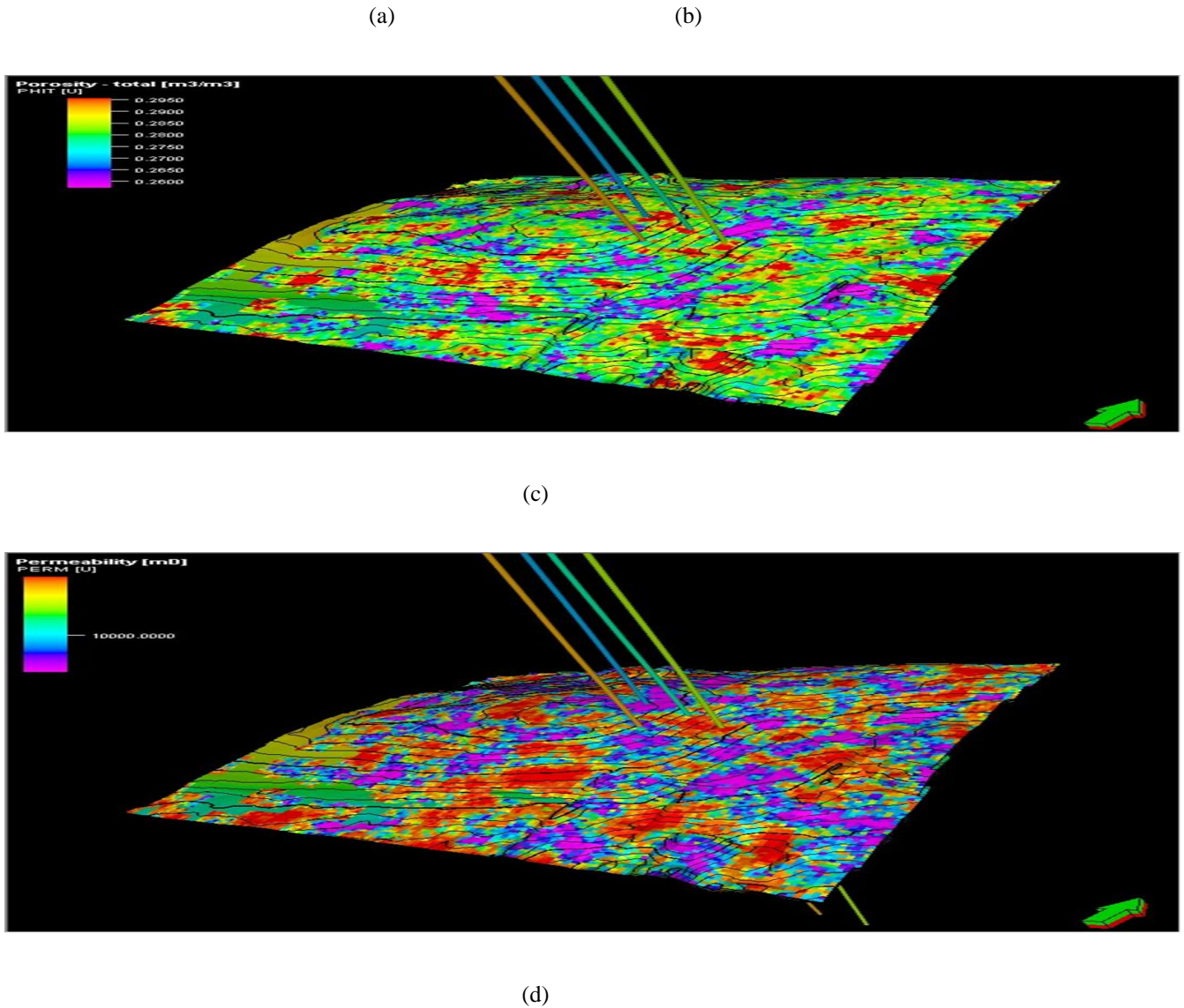
Figure 7: Showing Sand A (a): Depth structural Top Map (b) Depth structural Base Map (c) Modelled Porosity (d) Modelled Permeability.

From the porosity model, it is observed that the porosity ranges from 26% to 29%, and this corresponds to an extent with the range from the petrophysical analysis (23% to 28%). Also, the average porosity from the model is 27%, while that from the log was seen to be about 26%.

3.3   Rock Physics

Rock physics was carried out to quality check the Petrophysical analysis results, seismic interpretation, and modelling. The interpretation of the rock physics cross plots was made qualitatively. Cross-plots of various elastic parameters against some calculated Petrophysical parameters were generated. The cross-plots were carried out across the four wells of Sand A. the cross-plots were created on a rock physics template that included several models. The cross-plots that were generated using the developed template are listed below:

i) Poisson Ratio against Volume of shale for mapping lithology.

ii) Density against Primary Velocity for mapping lithology.

iii) Velocity Ratio against the acoustic impedance for mapping fluid content.

iv) Primary velocity against porosity for mapping degree of cementation.

3.3.1   Sand A Cross-Plots

Four cross-plots were generated for three wells across the entire reservoir using the produced template.

3.3.1.1   Well One

3.3.1.1.1 Poisson Ratio-Volume of Shale Cross-Plot

This cross-plot (Figure 8a) below was used to identify the lithologies within the reservoir. The plot revealed that the reservoir is predominantly characterized with low (blue to cyan colour) API values ranging from 25 to 75 API and Poisson ratio ranging from 0.25 to 0.45. Poisson ratio and API values of this range are diagnostic of sand units. Sediments with API values higher than about 100 are the shaly sediments. This supports the average volume of shale (0.245 units) obtained from the Petrophysical analysis of this well.

3.3.1.1.2   Density-Primary Velocity Cross-Plot

This cross-plot (Figure 8b) below described the lithology identified within the reservoir. From the plot, it could be observed that most of the sediments seemed to fall or align to the Gardner Sandstone line and within the Friable-Sand line, which shows that the reservoir is predominated by sand.

3.3.1.1.3   Velocity Ratio-Acoustic Impedance Cross- Pilot

This cross-plot revealed four different zones. The zones with the least density values (less than 2.15g/cm3) that are bluish indicate gas sands. The cyan characterizes the oil sands to yellow colour with their density values ranging from 2.15g/cm3 to about 2.3g/cm3. While the greenish zone having a density of about 2.45g/cm3 is indicating water-bearing sands. The last zone (red) has the highest density values above 2.45g/cm3 and is diagnostic of shale (Figure 8c).
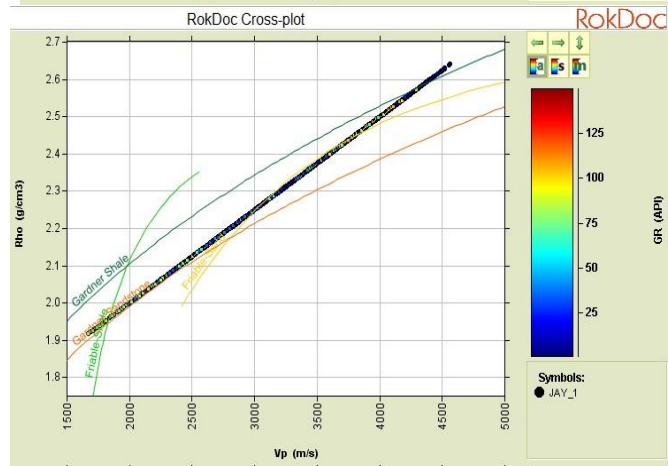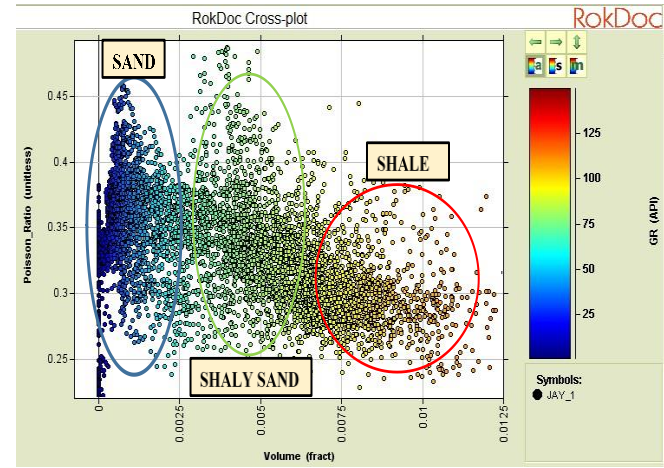
(a)   (b)
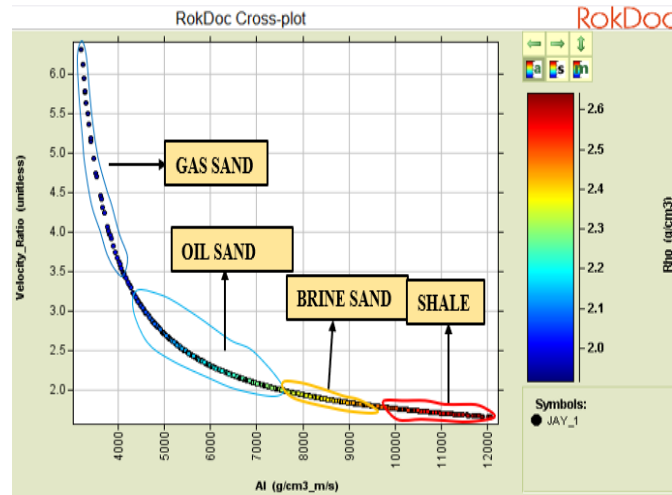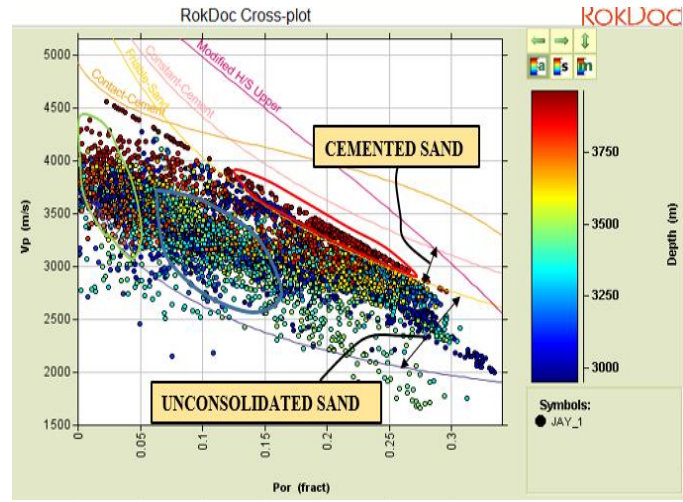
(c)   (d)
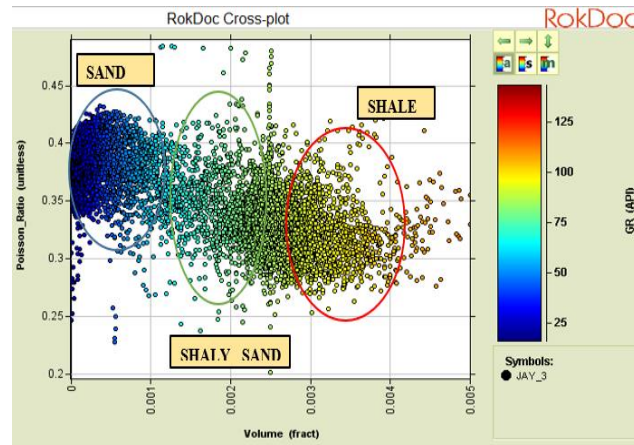
(e)   (f)
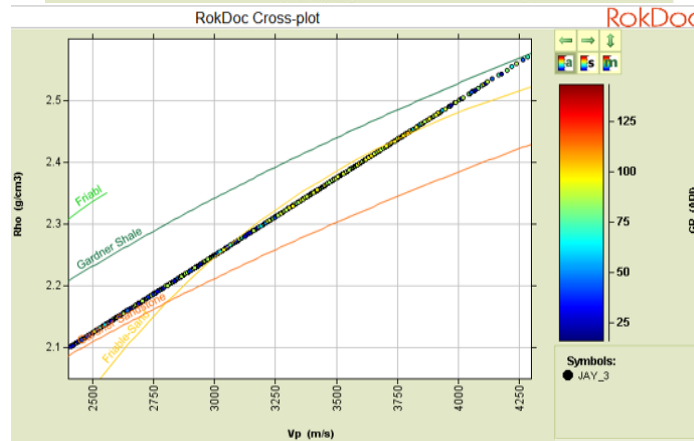
Figure 8: Showing Well 1 (a): Poisson Ratio Vs Shale Volume (b) Density Vs Primary Velocity (c) Velocity Ratio Vs   Acoustic Impedance (d) Primary Velocity Vs Porosity and Well 2 (e): Poisson Ratio Vs Shale Volume (f) Density Vs Primary Velocity.

3.3.1.1.4   Velocity-Porosity Cross-Plot

From the velocity-porosity cross-plot, it could be seen that the sediments coloured green, which occur at a depth of about 3500m, lies on and close to the Reuss lower bound, which implies that they are weak and unconsolidated. Their higher porosity values support this. Sediments also align to the Reuss bound's (a steeper part) which occurs at a depth of about 3600m, indicating that they are fractured. All of these sediments observed lie below the friable sand model, indicating that they are less cemented.

However, a small number of sediments was observed to lie above the friable model and beneath the Constant cement model at a higher depth, indicating that they are more compact than the upper part of this reservoir. This is shown in (Figure 8c).

3.3.1.2   Well Two

3.3.1.2.1   Poisson Ratio-Volume of Shale Cross-Plot

This cross-plot (Figure 8e) was used to delineate lithology for this well. From the plot, the sediments with low API values are predominant, which indicates sand. Those with API values of more than 100 are diagnostic of shales. The sand's API values vary from 25 to 75 API, as seen on the colour scale.

3.3.1.2.2   Density-Primary Velocity Cross-Plot

This cross-plot (Figure 8f) described the lithology identified within the reservoir. From the plot, it could be observed that most of the sediments seemed to fall or align to the Gardner Sandstone line.

3.3.1.2.3   Velocity Ratio-Acoustic Impedance Cross-Plot

Based on the velocity ratio (Vp/Vs)-Acoustic Impedance cross-plot in Figure 9a, the gas sand has the least values of density and acoustic impedance values, followed by the oil, water sand and the shale.

3.3.1.2.4   Velocity-Porosity Cross-Plot

From the velocity-porosity cross-plot, it could be seen that most of the sediments occur far above the Reuss lower bound but below the friable sand model. This is in agreement with the lithologies delineated by the Poisson Ratio-Volume of shale cross-plot (Figure 8f). This implies that the sediments in this well is more consolidated compared to well one (JAY1) and might have undergone geologic processes that give sediments strength (compaction, stress, digenesis etc.). The remaining sediments exist between the friable sand model and the Constant-Cement model which occur at deeper depths. This is shown in Figure 9b.

3.3.1.3   Well Three

3.3.1.3.1   Poisson Ratio-Volume of Shale Cross-Plot

This plot (Figure 9c) was used to identify the lithologies of the reservoir within this well. The plot revealed that the reservoir is predominantly characterized with low (blue to cyan colour) API values ranging from 25 to 75 API and Poisson ratio ranging from 0.25 to 0.45. This supports the small average volume of shale obtained from the Petrophysical analysis which is 0.005 units.

3.3.1.3.2 Density-Primary Porosity Cross-Plot

This cross-plot described the lithology identified within the reservoir. From the plot (Figure 9d), it could be observed that most of the sediments seemed to fall or align to the Gardner Sandstone model. Some other sediments also lie along and below the friable sand model which indicates that they are loose sediments. The sediments are far away from the Gardner Shale line which implies that it is predominantly sand.

3.3.1.3.3 Velocity Ratio-Acoustic Impedance Cross-Plot

This cross-plot revealed four distinguishable zones. The zones having the least density values (less than 2.15g/cm3) which are bluish is indicating gas sands which is the most predominant within this well. While the greenish zone having a density of about 2.45g/cm3 is indicating water-bearing sands. The last zone (red) has the highest density values which are above 2.45g/cm3 and thus diagnostic of shale. This is shown in Figure 9e below.

3.3.1.3.4 Velocity-Porosity Cross-Plot

This plot (Figure 9f) was similar to that obtained in well two. Most of the sediments occur below the friable sand model and thus shows that they are unconsolidated. Other few sediments are above the friable sand model indicating the occurrence of either mechanical or chemical compaction which are in greater depth.

4. Conclusion

This research work is aimed at characterizing the JAY field. The reason for an integrated study was to reduce risks and uncertainties associated with applying few methods in characterizing an inherently heterogeneous reservoir. The three methods utilized (seismic, Petrophysics and rock physics) all gave similar inferences in the characterization process and thus the objectives of carrying out this research work were achieved.

Maps generated for Sand A revealed structures that could enhance the accumulation of hydrocarbon which can be seen in the North-west central portion of the field. The trapping potential of the field can thus be attributed to faults and anticlines, acting either as fault assisted or anticline closures respectively. The rollover anticlines (orange portion) are found on structural high and formed on the downthrown block of the growth fault which indicate structural closures in these areas. It can be deduced from this study that the wells were located to target the anticlines. More productive zones were located further west of the existing wells via these structural maps, and porosity and permeability models.

The Petrophysical analysis indicated that the reservoirs have good pore interconnectivity (Average Øeffective =

24% & 21% and Average K_average = 9701md & 7737md for Sand A and B respectively.)

The rock physics analysis confirmed the result obtained from the Petrophysical analysis and furthermore, it showed that the lithologies within the reservoir were partially cemented and predominated by water then followed by gas which supports the high-water saturation obtained from the petrophysical analysis of the reservoir. This work thus highlighted the advantage of utilizing an integrated method in reservoir characterization.
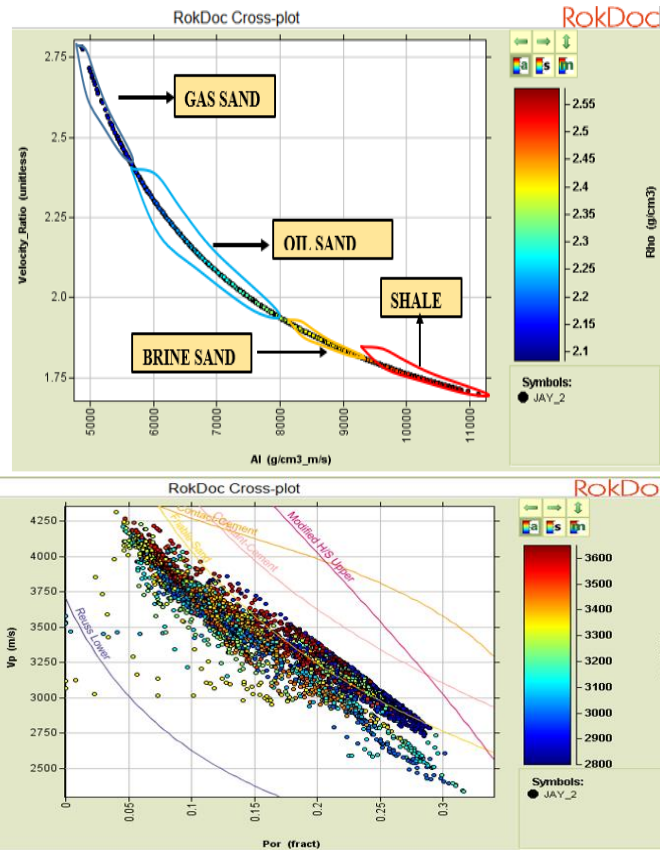
(a)   (b)
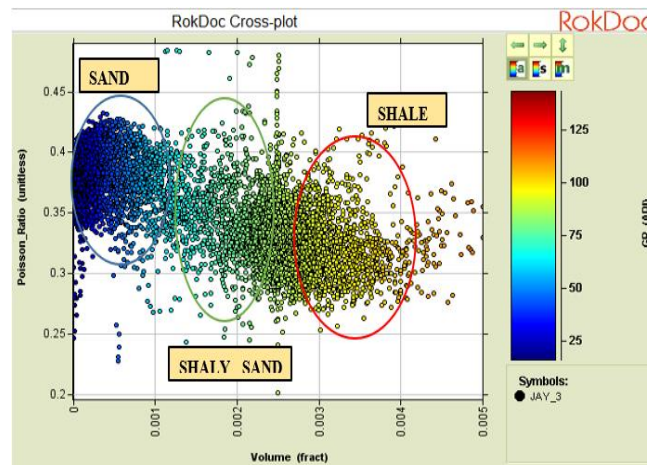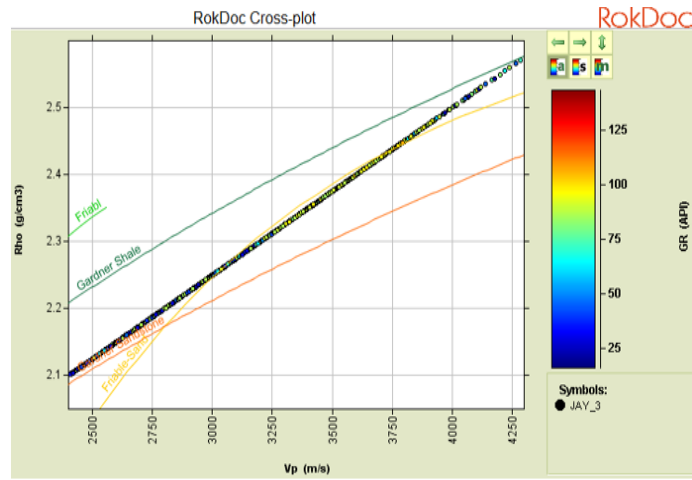
(c)   (d)
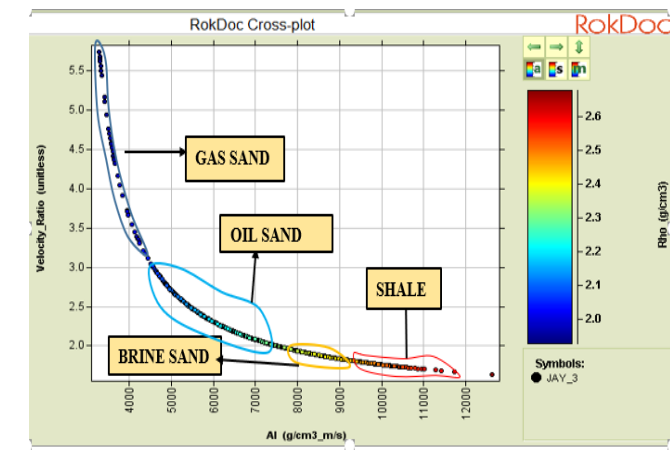
(e)   (f)
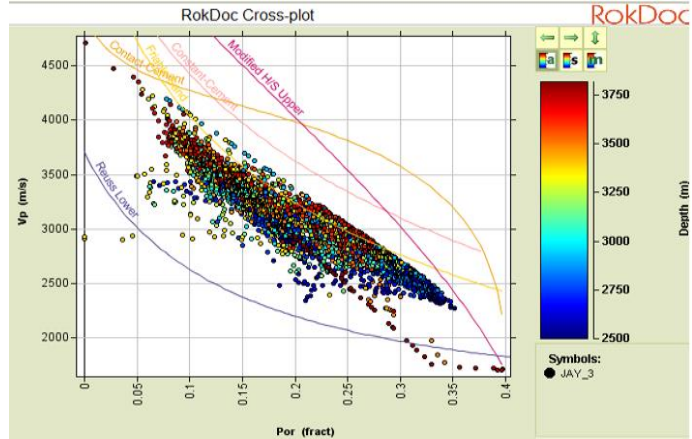
Figure 9: Showing Well 2 (a): Velocity Ratio Vs Acoustic Impedance (b) Primary Velocity Vs Porosity and Well 3 (c) Poisson Ratio Vs Shale Volume (d) Density Vs Primary Velocity (e): Velocity Ratio Vs   Acoustic Impedance (f) Primary Velocity Vs Porosity.

References

[1.] Abe, S. J. and Olowokere, M. T. (2013). Reservoir characterisation and formation evaluation of some parts of Niger Delta, using 3-D Seismic and well log data. Research journal in Engineering and Applied Sciences, 2 (4): 304-307.

[2.] Adaeze, I.U., Samuel, O.O. and Chukwuma, J.J. (2012). Petrophysical evaluation of Uzek well using well log and core data, offshore Depobelt, Niger Delta, Nigeria. Advances in Applied Science Research, 3(5): 2966-2991.

[3.] Ailin Jia, Dongbo He and Chengye Jia. (2012). Advances and Challenges of Reservoir Characterization: A Review of the Current State-of-the-Art. Earth Sciences, 1.

[4.] Amigun J. O. and. Bakare, N. O. (2013). Reservoir evaluation of "Danna" field Niger Delta using petrophysical analysis and 3-D seismic interpretation. Petroleum & Coal, 2 (55): 119-127.

[5.] Avbovbo, A. (1978). Tertiary lithostratigraphy of Niger Delta. American Association of Petroleum Geologists Bulletin,, 62: 295-300.

[6.] Avseth, P., Mavko, G. (2005). Quantitative seismic interpretation: Applying Rock Physics Tools to Reduce Interpretation Risk. Cambrdge University Presss.

[7.] Beka, F.T. and Oti, M.N. (1995). The distal offshore Niger Delta: frontier prospects of a mature petroleum province, in, Oti, M.N., and Postma, G. eds., Geology of Deltas. 237-241.

[8.] Berryman, J. G. (1980). Theory of Elastic Properties of Composite materials. Applied Pysics Letters.

[9.] Bustin, R. M. (1988). Sedimentology and characteristics of dispersed organic matter in Tertiary Niger Delta: origin of source rocks in a deltaic environment. American Association of Petroleum Geologists Bulletin, 72: 277-298.

[10.] Doust, H., and Omatsola, E., Niger Delta, in, Edwards, J. D., and Santogrossi, P.A., eds. (1990). Divergent/passive Margin Basins. AAPG Memoir 48: Tulsa, American Association of Petroleum Geologists, 239-248.

[11.] Edigbue, P.I., Komolafe, A.A., Adesida, A.A. and Itamuko, O.J. (2014). Hydrocarbon reservoir characterization of 'Keke' field, Niger Delta using 3-D seismic and petrophysical data . Standard Global Journal of Geology and Explorational Research, 1(2): 043-052.

[12.] Edwards, J. a. (1990). Summary and Conclusions, in, Edwards, J.D. and Santogrossi, P.A. ed., Divergent/passive Margin Basins. AAPG Memoir48: Tulsa, American Association of Petroleum Geologists, 239-248. .

[13.] Ejedawe, J. (1981). Patterns of incidence of oil reserves in Niger Delta Basin. American Association of Petroleum Geologists, 65: 1574-1585.

[14.] Ekweozor, C.M. and Okoye, N.V. (1980). Petroleum source-bed evaluation of Tertiary Niger Delta. American Association of Petroleum Geologists Bulletin, 64: 1251-1259.

[15.] Evamy, B.D., Haremboure, J., Kamerling, P., Knaap, W.A., Molloy, F.A. and Rowlands, P.H. (1978). Hydrocarbon habitat of tertiary Niger Delta. American Association of Petroleum Geologists Bulletin, 62: 277-298.

[16.] Frost, B. (November 16-19, 1997). A Cretaceous Niger Delta Petroleum System, in, Extended Abstract AAPG/ABGP Hedberg Research Symposium. Petroleum Systems of the South Atlantic Margin. Rio de

Janeiro, Brazil.

[17.] Gassmann, F. (1951). Uber die elastizit¨ ¨ at por ¨oser medien. Vierteljahrss chrift der Naturforschenden Gesellschaft in Zurich, 96, 1–23.

[18.] Gommesen, L., G. Mavko, T. Mukerji and I.L. Fabricius. (October 6-11, 2002). Fluid substitution studies for North Sea chalk logging data. Proceedings of the SEG Annual Meeting. Salt Lake City, Utah.

[19.] Haack, R.C., Sundararaman, P. and Dahl, J. (1997). (November 16-19, 1997). Niger Delta petroleum System, in,Extended Abstracts, . AAPG/ABGP Hedberg Research Symposium. Rio de Janeiro, Brazil: Petroleum Systems of the South Atlantic Margin.

[20.] Hospers, J. (1965). Gravity field and structure of the Niger Delta, Nigeria, West Africa. Geological Society of American Bulletin, v. 76, p. 407-422.

[21.] Hunt, J. (1990). Generation and migration of petroleum from abnormally pressured fluid compartments. American Association of Petroleum Geologists Bulletin, 74: 1-12.

[22.] Ihianle O. E., Alile O.M., Azi, S. O., Airen J. O. and Osuoji O. U. (2013). Three dimensional seismic/well logs and structural interpretation over 'X – Y' field in the Niger Delta area of Nigeria. Science and Technology, 2(3): 47-54.

[23.] Kaplan, A., Lusser, C.U., Norton, I.O. (1994). Tectonic map of the world, panel 10: Tulsa. American Association of Petroleum Geologists, scale 1:10,000,000.

[24.] Keary, P., Brook, M. and Hill, I. (2002). An Introduction to Geophysical Exploration. Oxford, Blackwell scientific publication.

[25.] Klett, T. A. (1997). Ranking of the world's oil and gas provinces by known petroleum volumes. U.S. Geological Survey Open-file Report-97-463, CD-ROM.

[26.] Kulke, H., 1995, Nigeria, in, Kulke, H., ed. (1995). Regional Petroleum Geology of the World. Part II: Africa, America, Australia and Antarctica (pp. 143-172). Berlin: Gebrüder Borntraeger.

[27.] Lambert-Aikhionbare, D. O. and Ibe, A.C. (1984). Petroleum source-bed evaluation of the Tertiary Niger Delta: discussion. American Association of Petroleum Geologists Bulletin, 68: 387-394.

[28.] Lehner, P. and De Ruiter, P.A.C. (1977). Structural history of Atlantic margin of Africa. American Association of Petroleum Geologists Bulletin, 61: 961-981.

[29.] Lowrie, W. (2007). Fundamentals of geophysics. New York: Cambridge University press.

[30.] Mondol, H. (2010). Seismic Exploration. Petroleum Geoscience, , 375–402.

[31.] Nwachukwu, J.I. and Chukwurah, P.I. (1986). Organic matter of Agbada formationOrganic matter of Agbada formation Niger Delta, Nigeria. American Association of Petroleum Geologists Bulletin, 70: 48-55.

[32.] Richard J. O'Connell Bernard Budiansky. (1974). Seismic velocities in dry and saturated cracked solids. Journal of Geophysical research, 5412-5416.

[33.] Short, K.C. and Stauble, J. (1967). Outline geology of the Niger Delta. AAPG Bull5, 761–779.

[34.] Slatt, R., and S. Mark. (2002). Practical reservoir characterization for the independent operator,computer technology for comprehensive reservoir characterization:. Petroleum Technology Transfer Council, 512-514.

[35.] Stacher, P. (1995). Present understanding of the Niger Delta hydrocarbon habitat, in, Oti M.N., and

Postma, G., eds. Geology of Deltas: Rotterdam, A.A. Balkema, 257-267.

[36.] Weber, K. (1978). Hydrocarbon distribution patterns in Nigerian growth fault structures controlled by structural style and stratigraphy. Journal of Petroleum Science and Engineering, 1: 91-104.

[37.] Weber, K.J. and Daukoru, E.M. (1975). Petroleum Geology of the Niger Delta. Proceedings of the Ninth World Petroleum Congress volume 2, Geology (pp. 210-221). London: Applied Science Publishers, Ltd.